

Enhanced Change-Point Detection in Functional Means

Shuhao Jiao*, Ngai Hang Chan, and Chun Yip Yau

*Department of Statistics,
The Chinese University of Hong Kong,
Shatin NT, Hong Kong*

Abstract

A new dimension reduction method for change-point detection in functional means is developed in this paper. The major advantage and novelty of the proposed method is its efficiency in selecting basis functions that capture the change/jump of functional means, leading to a higher detection power, especially when the functions cannot be sufficiently explained by a small number of basis functions or are contaminated by random noises. The theoretical results demonstrate that even when the change shrinks to zero, the proposed approach can still detect the change asymptotically almost surely. The numerical simulation studies justify the superiority of the proposed approach compared to the method based on functional principal components and the fully functional approach without dimension reduction. An application to annual humidity trajectories illustrates the practical superiority of the developed approach.

Key words: Change point analysis, Dimension reduction, Enhanced detection, Functional Mean, Functional data analysis, Weakly dependent functional data.

1 Introduction

This paper provides a new method to tackle a popular problem in functional data analysis, detecting the change point in functional means of a sequence of functional time series. The general setting is that a single change point partitions the entire sequence into two local stationary blocks, where the functions in each block share the same mean function.

*Corresponding Author: shuhaojiao@cuhk.edu.hk

There have been a number of methods developed for functional structural breaks in the mean function. Many of them are developed based on dimension reduction or projection. A typical step in such projection-based approaches is to project the functions onto a finite number of orthonormal basis functions, and the projection scores are employed to detect the change in mean of independent or dependent functional data sequence. See, for example, Berkes *et al.* (2009), Aue *et al.* (2009), Zhang *et al.* (2011), Aston and Kirch (2012a) and the references therein. More recently, Fremdt *et al.* (2014) consider structural break detection by using functional principal component analysis (FPCA) under an increasing number of projections. Dimension reduction is also utilized to detect change points of multivariate functions under separability assumptions (e.g., spatial temporal data or brain image data), see Aston and Kirch (2012b), Gromenko *et al.* (2017) and Stoehr *et al.* (2021). Structural break detection in the coefficient operators of functional linear models is considered in Aue *et al.* (2014). Structural break detection in spectrum and trace of covariance operator is studied in Jaruskova (2013) and Aue *et al.* (2020). Test of stationarity of functional time series in spectral domain is developed in Aue and van Delft (2020).

In the change-point analysis of functional data, one major limitation of dimension reduction is that, when the selected basis functions are not aligned with the jump of mean function, the projection-based detector fails to detect the change points. To solve this problem, an alternative fully functional approach is employed in Horváth *et al.* (2014), Aue *et al.* (2018) and Jiao *et al.* (2022), which does not rely on any dimension reduction. In the fully functional detection procedure, the null distribution involves infinitely many unknown parameters and requires additional truncation step, however. To circumvent this difficulty, Sharipov *et al.* (2016) and Buccia and Wendler (2017) study the bootstrap procedure. In addition to fully functional approach, a change-aligned method is considered in Torgovitski (2015).

Although the fully functional detector is guaranteed to detect the change as the sample size diverges, one major limitation of such approach is that it incorporates all basis functions that span the functional space, including potentially infinitely many irrelevant (unaligned with the change) basis functions. The irrelevant basis functions do not contribute to change point detection, and can potentially lead to loss of detection power due to their nuisance effect. In the literature, sample trajectories are often pre-smoothed with a few smooth basis functions. In that case, the fully functional approach also perform decently for the smoothed functions, since the nuisance effect is significantly attenuated by functional smoothing, and thus is not very substantial when the number of pre-smoothing basis is small. Pre-smoothing can lead to serious loss of information, however. It will make the fully functional detector fail when the functions are smoothed with low-frequency basis when the change functions are driven by high frequencies. Therefore, it is more advantageous to select basis functions which are informative to the change of mean, than to incorporate all basis functions or smooth the functions with pre-specified basis.

In this paper, we develop a new detection method for structural breaks in functional means. The key idea is to align the selected basis functions with the change of mean

function. To achieve this goal, we introduce a discrepancy enhanced covariance (DEC) operator, of which the eigenfunctions constitute the basis functions for dimension reduction. The DEC operator involves two parts. The first part is the long-run covariance and the second part is the enhancement term, which is calibrated to magnify the influence of the change-aligned basis functions. These basis functions have the advantages that they are able to align with the jump function. Unlike the fully functional approach, the null distribution of the developed detector only involves a finite number of parameters, and the nuisance effect of unaligned/irrelevant basis functions is substantially reduced. Another contribution of this paper is that we investigate the detection power under more complicated settings. Specifically, we allow both the change magnitude and dimension to change with the sample size. It is proved that the power of the proposed detector can still approach one as the sample size goes to infinity, even when the change magnitude diminishes. The asymptotic properties of the discrepancy enhanced covariance operator and change point detector are also thoroughly studied under both null and alternative hypothesis.

The rest of the article is organized as follows. In Section 2, we present the developed enhanced detection procedure and the implementation details. Selection of tuning parameters and theoretical results are discussed in Section 3. In Section 4, we report the simulation results under different settings. In Section 5, we present the real data analysis on annual humidity trajectories. The paper is concluded in Section 6. Proofs are given in the online supplementary material.

2 Enhanced Detection Procedure

In this paper, a single structural break problem is considered. When there are multiple change-points, we propose to apply some localization method to segment the whole sequence into multiple blocks, where at most one change-point (AMOC) assumption is made for each block, and then use the proposed approach to each block to detect the change-point. Backward elimination can be applied to refine the detection. More details can be found in the real data analysis of humidity trajectories. Because this is beyond the scope of this paper, we do not pursue it in details here.

2.1 Projection-based Detector

A single change-point model can be formulated as

$$X_n(t) = \begin{cases} \mu_0(t) + e_n(t), & n \leq k^*, \\ \mu_1(t) + e_n(t), & n > k^*, \end{cases} \quad (2-1)$$

where $k^* = \lfloor N\theta^* \rfloor$, and the zero-mean random functions $\{e_n: n \in \mathbb{N}\}$ take realizations in $L^2[0, 1]$ and satisfy that $E \int e_n^2(t) dt < \infty$. In the space $L^2[0, 1]$, the inner product

of two elements x, y are defined as $\langle x, y \rangle = \int_0^1 x(t)y(t)dt$ and the norm is defined as $\|x\|^2 = \int_0^1 x^2(t)dt < \infty$. It is assumed that $\{e_n: n \in \mathbb{N}\}$ are weakly dependent as quantified in the following assumption.

Assumption 1. There is a measurable function $f: S^\infty \rightarrow L^2[0, 1]$, where S is a measurable space, and *i.i.d.* innovations $\{\epsilon_n: n \in \mathbb{N}\}$ take values in S , so that $e_n(t) = f(\epsilon_n, \epsilon_{n-1}, \dots)$. In addition, there exists a m -dependent sequence $\{e_{n,m}(t): i \in \mathbb{N}\}$, so that $e_{n,m}(t) = f(\epsilon_n, \dots, \epsilon_{n-m+1}, \epsilon_{n-m}^*, \epsilon_{n-m-1}^*, \dots)$, where ϵ_n^* is an independent copy of ϵ_n , such that $\sum_{m=0}^{\infty} \{E\|e_n(t) - e_{n,m}(t)\|^p\}^{1/p} < \infty$ for some $p > 2$.

The goal is to detect whether a change point exists and identify the location of the change-point. Define the jump function as $\delta(t) = \mu_0(t) - \mu_1(t)$, and the following test is implemented to detect the change point,

$$H_0: \delta(t) = 0 \quad \text{vs} \quad H_a: \delta(t) \neq 0. \quad (2-2)$$

Given a sequence of orthonormal basis functions $\{\nu_d(t): d = 1, \dots, D\}$, define $\eta_{nd} = \langle X_n, \nu_d \rangle$ and $\boldsymbol{\eta}_n = (\eta_{nd}, \dots, \eta_{nD})'$, and the cumulative summation (CUSUM) as

$$\mathbf{S}_{N,\theta} = \sum_{n=1}^{\lfloor N\theta \rfloor} \boldsymbol{\eta}_n - \theta \sum_{n=1}^N \boldsymbol{\eta}_n.$$

The projection-based method is based on the squared CUSUM statistics,

$$T_N(\theta) = N^{-1} \|\mathbf{S}_{N,\theta}\|_2^2, \quad (2-3)$$

where $\|\cdot\|_2$ denotes the ℓ^2 -norm. The value of $T_N(\theta)$ should tend to be large at the true change point θ^* , thus by convention, the following max-type quantity is employed as the detector of change point

$$T_N(\hat{\theta}_N^*) = \max_{0 < \theta < 1} T_N(\theta),$$

and for uniqueness, the infimum of the maximizers of $T_N(\theta)$, namely

$$\hat{\theta}_N^* = \inf\{\theta: T_N(\theta) = \sup_{\theta' \in (0,1)} T_N(\theta')\}$$

is assumed to be the change point candidate. In principle, it is desirable for the selected basis functions $\{\nu_d(t): d = 1, \dots, D\}$ to capture the jump function, say, $\langle \nu_d, \delta \rangle \neq 0$ for some d . Otherwise, the method fails even if $\|\delta\|$ is much bigger than zero.

The following result quantifies the null distribution of the projection-based detector.

Theorem 1. Under Assumption 1 and $H_0: \delta(t) = 0$,

$$T_N(\hat{\theta}_N^*) \xrightarrow{d} \sup_{\theta \in (0,1)} \mathbf{B}'(\theta) \Sigma_D \mathbf{B}(\theta),$$

where $\mathbf{B}(\theta) = (B_1(\theta), \dots, B_D(\theta))'$ and $\{B_d(\theta): d \geq 1\}$ are *i.i.d.* Brownian bridges and $\Sigma_D = \sum_{h=-\infty}^{\infty} \text{Cov}(\boldsymbol{\eta}_n \boldsymbol{\eta}_{n+h})$.

The theorem follows from Theorem A.1 in Aue *et al.* (2009). Theorem 1 asymptotically validates the test of H_0 . Specifically, H_0 is rejected if the test statistic $T_N(\hat{\theta}_N^*)$ exceeds the corresponding quantile of the null distribution $\sup_{\theta \in (0,1)} \mathbf{B}'(\theta) \Sigma_D \mathbf{B}(\theta)$.

2.2 Selection of Basis Functions

Define the (auto)covariance function of $\{X_n: n \in \mathbb{N}\}$ as $C_{X,h}(t, s) = E\{e_n(t)e_{n+h}(s)\}$, and the long-run covariance as $LC_X(t, s) = \sum_{h=-\infty}^{\infty} C_{X,h}(t, s)$. With a sequence of positive eigenvalues $\{\tau_d: d \geq 1\}$ and orthonormal eigenfunctions $\{\phi_d(t): d \geq 1\}$, the spectral decomposition $LC_X(t, s) = \sum_{d \geq 1} \tau_d \phi_d(t) \phi_d(s)$ is allowed.

The selection of $\{\nu_d(t): d = 1, \dots, D\}$ highly influences the performance of the detector. A popular way of selecting the basis functions is to employ the major eigenfunctions of the (long-run) covariance operator $\mathcal{LC}_X(\cdot)$, induced by the kernel $LC_X(t, s)$, and the resulting null distribution is $\sup_{\theta \in (0,1)} \sum_{d=1}^D \tau_d B_d^2(\theta)$ (see Berkes *et al.* (2009), Hörmann *et al.* (2015) and Torgovitski (2015)). Such basis functions are not guaranteed to align with $\delta(t)$. To solve this problem, the developed approach is based on the major eigenfunctions of the discrepancy enhanced covariance (DEC) operator described as follows.

To separate the jump-aligned component and other irrelevant components for selecting tuning parameters (see Section 3.1), first transform the functions as follows:

$$Y_n^{(\kappa)}(t) = X_n(t) - \left\langle X_n, \frac{\delta}{\|\delta\| + \kappa} \right\rangle \frac{\delta(t)}{\|\delta\| + \kappa}, \quad (2-4)$$

where κ is a small-valued positive tuning parameter shrinking to zero as $N \rightarrow \infty$. Note that $\delta(t)$ is typically unknown, and the estimation of $\delta(t)$ will be discussed later. The term $Y_n^{(\kappa)}(t)$ in (2-4) is well defined under both H_0 and H_a . The DEC is defined as

$$K^{(\kappa)}(t, s) = LC_{Y,\kappa}(t, s) + \rho \delta(t) \delta(s),$$

where ρ is the enhancement parameter to be specified. The quantity $LC_{Y,\kappa}(t, s)$ is the long-run covariance of $Y_n^{(\kappa)}(t)$, defined as

$$LC_{Y,\kappa}(t, s) = \sum_{h=-\infty}^{\infty} C_{Y,h}^{(\kappa)}(t, s),$$

where $C_{Y,h}^{(\kappa)}(t, s) = \text{cov}\{Y_n^{(\kappa)}(t), Y_{n+h}^{(\kappa)}(s)\} = E\{Y_n^{(\kappa)}(t) - EY_n^{(\kappa)}(t)\} \{Y_{n+h}^{(\kappa)}(s) - EY_{n+h}^{(\kappa)}(s)\}$. By Mercer's theorem, suppose that a sequence of decreasing non-negative eigenvalues $\{\theta_d^{(\kappa)}: d \geq 1\}$ and a sequence of corresponding orthonormal eigenfunctions $\{\psi_d^{(\kappa)}: d \geq 1\}$ can be found such that

$$K^{(\kappa)}(t, s) = \sum_{d \geq 1} \theta_d^{(\kappa)} \psi_d^{(\kappa)}(t) \psi_d^{(\kappa)}(s).$$

It is proposed to make use of $\{\psi_d^{(\kappa)}(t): d = 1, \dots, D\}$ in defining the test statistic in (2-3). The quantity D is selected by an adjusted variance percentage criterion, and the details are in Section 3.1.3.

To understand this selection procedure, note that under H_a , first define $K(t, s) = LC_Y(t, s) + \rho\delta(t)\delta(s)$, where

$$LC_Y(t, s) = \sum_{h=-\infty}^{\infty} C_{Y,h}(t, s) = \sum_{h=-\infty}^{\infty} E\{Y_n(t) - EY_n(t)\}\{Y_{n+h}(s) - EY_{n+h}(s)\}$$

and $\{Y_n(t): n \in \mathbb{N}\}$ are defined as

$$Y_n(t) = X_n(t) - \left\langle X_n, \frac{\delta}{\|\delta\|} \right\rangle \frac{\delta(t)}{\|\delta\|}. \quad (2-5)$$

The kernel function $K(t, s)$ is positive definite, thus similar to $K^{(\kappa)}(t, s)$, the spectral decomposition can be found as $K(t, s) = \sum_{d \geq 1} \theta_d \psi_d(t) \psi_d(s)$.

Evidently, under H_a and as $\kappa \rightarrow 0$, $LC_{Y,\kappa} \rightarrow LC_Y$, and therefore, $\{(\theta_d^{(\kappa)}, \psi_d^{(\kappa)}(t)): d \geq 1\}$ converge to $\{(\theta_d, \psi_d(t)): d \geq 1\}$. Clearly, $\delta(t)$ is orthogonal to all the eigenfunctions of $LC_Y(\cdot)$ due to the projection (2-5), and thus $\{\rho\|\delta\|^2, \delta(t)/\|\delta\|\}$ is a pair of eigenvalue and eigenfunction of $K(t, s)$. In what follows, it is supposed that $\theta_{d^*} = \rho\|\delta\|^2$ and $\psi_{d^*}(t) = \delta(t)/\|\delta\|$, and denote $\theta_{d^*}^{(\kappa)}$ and $\psi_{d^*}^{(\kappa)}(t)$ as the counterparts of $K^{(\kappa)}(t, s)$.

Observe that $\psi_{d^*}(t) = \delta(t)/\|\delta\|$ is the only eigenfunction of $K(t, s)$ aligned with the jump function $\delta(t)$, and a large value of ρ leads to large eigenvalue $\rho\|\delta\|^2$. Then by the adjusted variance percentage criterion in Section 3.1.3, the eigenfunction $\delta(t)/\|\delta\|$ is very likely to be selected with a sufficient large ρ . In practice, $\delta(t)$ is typically unknown and $K(t, s)$ may be not well-defined, thus it is of immense interest to enhance the influence of the jump-aligned counterpart of $K^{(\kappa)}(t, s)$, namely, $\psi_{d^*}^{(\kappa)}(t)$. If $\delta(t) = 0$, then $K^{(\kappa)}(t, s)$ is equivalent to $LC_X(t, s)$, and the null distribution is equivalent to the conventional counterpart based on the functional principal components of $LC_X(t, s)$. In the following, $\psi_{d^*}^{(\kappa)}$ is termed as *jump-aligned basis*.

Remark 1. An alternative approach is to employ the major functional principal components of $LC_X(t, s) + \rho\delta(t)\delta(s)$. While this is also reasonable, we still recommend to use the projection step (2-5) first. The reason is that it is easier to tune the eigenvalue spacing after projection, which highly influences the identifiability and estimation accuracy of eigenfunctions (see e.g., Corollary 1.6 in Gohberg *et al.* (1990)). More details are given in Section 3.1.2. In addition, without projection, we need to find all aligned (not orthogonal to $\delta(t)$) eigenfunctions of $LC_X(t, s) + \rho\delta(t)\delta(s)$ to check if ρ is sufficiently large, making the selection of tuning parameters much more complicated.

2.3 Estimations

Since the limiting distribution under H_0 depends on the first D eigenfunctions of $K^{(\kappa)}(t, s)$, one key step is to estimate $K^{(\kappa)}(t, s)$. First, we discuss the estimation of

$\delta(t)$. We propose to select some fixed grids $\{n_i: i \in G\} \subset (0, N)^{\aleph G}$, where $\aleph G$ is the cardinality of the set G , and for each grid, define

$$\hat{\delta}_{n_i}(t) = \frac{1}{n_i} \sum_{n=1}^{n_i} X_n(t) - \frac{1}{N - n_i} \sum_{n=n_i+1}^N X_n(t).$$

and the estimation of $\delta(t)$ is given by $\hat{\delta}(t) = (\aleph G)^{-1} \sum_{n_i \in G} \hat{\delta}_{n_i}(t)$. Observe that, under H_a , $E\{\hat{\delta}(t)\}/\delta(t) = C(\theta^*) \leq 1$, where $C(\theta^*)$ is a constant related to θ^* , and the equality holds when $\aleph G = 1$ and the selected grid is exactly k^* . Although $\hat{\delta}(t)$ is not a consistent estimator of $\delta(t)$, this is not an issue in our approach. A goal here is to find the basis functions that are aligned with the jump function. In other words, the shape rather than the magnitude of $\delta(t)$ is of the major interest. By continuous mapping theorem, $\hat{\delta}/\|\hat{\delta}\| \xrightarrow{P} E\hat{\delta}/\|E\hat{\delta}\| = \delta/\|\delta\|$, and the enhancement term $\rho\delta(t)\delta(s)$ is equivalent to $C^2(\theta^*)\rho\{C^{-2}(\theta^*)\delta(t)\delta(s)\}$. Thus the non-consistency of estimation does not lead to any loss of information.

Then we construct $Y_n^{(\kappa)}(t)$ as

$$Y_n^{(\kappa)}(t) = X_n(t) - \left\langle X_n, \frac{\hat{\delta}}{\|\hat{\delta}\| + \kappa} \right\rangle \frac{\hat{\delta}(t)}{\|\hat{\delta}\| + \kappa}.$$

Further this leads to the empirical (auto)covariance of $\{Y_n^{(\kappa)}(t): n \in \mathbb{N}\}$ displayed below

$$\begin{aligned} \hat{C}_{Y,h}^{(\kappa)}(t, s) &= \frac{1}{N - h} \sum_{n=1}^{N-h} \{Y_n^{(\kappa)}(t) - \bar{Y}_n^{(\kappa)}(t)\} \{Y_{n+h}^{(\kappa)}(s) - \bar{Y}_{n+h}^{(\kappa)}(s)\}, \quad h \geq 0, \\ \hat{C}_{Y,h}^{(\kappa)}(t, s) &= \frac{1}{N + h} \sum_{n=|h|+1}^N \{Y_n^{(\kappa)}(t) - \bar{Y}_n^{(\kappa)}(t)\} \{Y_{n+h}^{(\kappa)}(s) - \bar{Y}_{n+h}^{(\kappa)}(s)\}, \quad h < 0, \end{aligned}$$

where

$$\bar{Y}_n^{(\kappa)}(t) = \begin{cases} \frac{1}{\hat{k}_N^{(f)}} \sum_{j=1}^{\hat{k}_N^{(f)}} Y_j^{(\kappa)}(t), & 1 \leq n \leq \hat{k}_N^{(f)}, \\ \frac{1}{N - \hat{k}_N^{(f)}} \sum_{j=\hat{k}_N^{(f)}+1}^N Y_j^{(\kappa)}(t), & \hat{k}_N^{(f)} + 1 \leq n \leq N, \end{cases}$$

and $\hat{k}_N^{(f)}$ is defined as the infimum of the the maximizer(s) of the following quantity

$$M(k) = \frac{1}{N} \int \left(\sum_{n=1}^k X_n(t) - \frac{k}{N} \sum_{n=1}^N X_n(t) \right)^2 dt.$$

The estimation of $K^{(\kappa)}(t, s)$ is then given as follows,

$$\hat{K}^{(\kappa)}(t, s) = \sum_{h=-\ell}^{\ell} W\left(\frac{h}{\ell}\right) \hat{C}_{Y,h}^{(\kappa)}(t, s) + \rho\hat{\delta}(t)\hat{\delta}(s),$$

and the kernel function $W(\cdot)$ satisfies the following assumptions.

Assumption 2. $c_1^{-1}|u|^{\alpha_w} \leq 1 - W(u) \leq c_1|u|^{\alpha_w}$, $W(0) = 1$, $0 \leq W(\cdot) \leq 1$, $W(u) = W(-u)$, $W(u) = 0$ if $|u| > 1$, and the bandwidth ℓ satisfies $\ell = O(N^{\alpha_\ell})$, where $0 < \alpha_\ell < 1/2$.

The corresponding empirical eigenfunctions are defined through the eigen-equation $\widehat{K}^{(\kappa)}(\widehat{\psi}_d^{(\kappa)})(t) = \widehat{\theta}_d^{(\kappa)}\widehat{\psi}_d^{(\kappa)}(t)$, leading to $\widehat{\boldsymbol{\eta}}_n = (\widehat{\eta}_{n1}, \dots, \widehat{\eta}_{nD})'$, where $\widehat{\eta}_{nd} = \langle X_n, \widehat{\psi}_d^{(\kappa)} \rangle$ and $\widehat{\mathbf{S}}_{N,\theta} = \sum_{n=1}^{\lfloor N\theta \rfloor} \widehat{\boldsymbol{\eta}}_d - \theta \sum_{n=1}^N \widehat{\boldsymbol{\eta}}_d$. Similarly, Σ_D is estimated with the kernel estimator

$$\widehat{\Sigma}_D = \sum_{h=-\ell}^{\ell} W\left(\frac{h}{\ell}\right) \widehat{C}_{\eta,h},$$

where $\widehat{C}_{\eta,h}$ is defined similar to $\widehat{C}_{Y,h}^{(\kappa)}$ with $Y_n^{(\kappa)}(t)$ replaced by $\widehat{\boldsymbol{\eta}}_n$. The estimated detector is obtained as $\widetilde{T}_N(\theta) = N^{-1} \|\widehat{\mathbf{S}}_{N,\theta}\|_2^2$.

3 Discussion on the Selection of Tuning Parameters and Power Studies

3.1 Selection of Tuning Parameters

3.1.1 Selection of ρ

Typically a large value of ρ can substantially bring forward the rank of the jump-aligned basis $\psi_{d^*}^{(\kappa)}(t)$ in the sequence $\{\psi_d^{(\kappa)}: d \geq 1\}$, making it easier to be selected, and meanwhile more irrelevant basis functions are truncated to eliminate more nuisance effect. However, it is not always advantageous to select a very large value of ρ . The reason is that the empirical enhancement term $\rho\widehat{\delta}(t)\widehat{\delta}(s)$ is always non-zero due to the estimation error, and under H_0 the estimation error of the term may lead to high type-I error if ρ is selected overly large. Therefore, in principle, it is ideal that the enhancement term $\rho\widehat{\delta}(t)\widehat{\delta}(s)$ lays asymptotically trivial influence on the convergence of $\widehat{K}^{(\kappa)}(t, s)$ under H_0 . To achieve this goal, ρ should be selected so that $\rho\widehat{\delta}(t)\widehat{\delta}(s)$ converges to zero faster than $\widehat{LC}_{Y,\kappa}(t, s) - LC_X(t, s)$. Under Assumption 1 and H_0 , it can be shown that $\widehat{\delta} = O_p(N^{-1/2})$. Suppose that the convergence rate of $\widehat{LC}_{Y,\kappa}(t, s)$ under H_0 is $O_p(N^{-r_0})$, then ρ should be selected so that $N^{r_0-1}\rho \rightarrow 0$. It will be shown in the simulation section that the performance of the detector is robust to the selection of ρ .

To quantify r_0 , we make use of the following notations. The quantity “const.” represents a positive constant and $\|\cdot\|_S$ signifies the Hilbert-Schmidt norm.

Assumption 3. There exist $\alpha_c, \alpha_\kappa > 0$, so that $\|C_{X,h}\|_2 \leq \text{const.}h^{-\alpha_c}$ and $\kappa = O(N^{-\alpha_\kappa})$.

The following theorem quantifies the convergence rate of the estimated long-run covariance operator $\widehat{\mathcal{LC}}_{Y,\kappa}(\cdot)$ induced by $\widehat{LC}_{Y,\kappa}(t, s)$.

Theorem 2. Under Assumption 1, 2 and 3, if H_0 is true and $N^{-1}\ell\kappa^{-2} \rightarrow 0$, then for arbitrary small $\epsilon > 0$,

$$\|\widehat{\mathcal{LC}}_{Y,\kappa} - \mathcal{LC}_X\|_{\mathcal{S}} \leq O_p(1)N^{\max\{\alpha_\ell-1/2, -(\alpha_c-1)/\alpha_\ell, -1+2\alpha_\kappa+\alpha_\ell\}} \\ \vee \begin{cases} N^{-(\alpha_c-1)\alpha_\ell}, & \text{if } \alpha_w - \alpha_c > -1. \\ N^{-(\alpha_c-1)\alpha_\ell+\epsilon}, & \text{if } \alpha_w - \alpha_c = -1. \\ N^{-\alpha_w\alpha_\ell}, & \text{if } \alpha_w - \alpha_c < -1. \end{cases}$$

Moreover, if H_a is true and $\ell\kappa\|\delta\|^{-1} \rightarrow 0$, then for arbitrary small $\epsilon > 0$,

$$\|\widehat{\mathcal{LC}}_{Y,\kappa} - \mathcal{LC}_Y\|_{\mathcal{S}} \leq O_p(1)N^{\max\{\alpha_\ell-1/2, -(\alpha_c-1)/\alpha_\ell, \alpha_\ell-\alpha_\kappa-\alpha_\delta\}} \\ \vee \begin{cases} N^{-(\alpha_c-1)\alpha_\ell}, & \text{if } \alpha_w - \alpha_c > -1. \\ N^{-(\alpha_c-1)\alpha_\ell+\epsilon}, & \text{if } \alpha_w - \alpha_c = -1. \\ N^{-\alpha_w\alpha_\ell}, & \text{if } \alpha_w - \alpha_c < -1. \end{cases}$$

Theorem 2 gives the convergence rate of $\widehat{\mathcal{LC}}_{Y,\kappa}$ under both H_0 and H_a . The convergence rate is specified through multiple parameters. To simplify the notations, r_0 is denoted as the convergence rate of $\widehat{\mathcal{LC}}_{Y,\kappa}$ under H_0 , and r_a is denoted as the convergence rate of $\widehat{\mathcal{LC}}_{Y,\kappa}$ under H_a . The parameters α_w and α_c are unknown, but can be approximated by fitting a geometrically decaying function $f_{c,\alpha}(h) = ch^\alpha$ to $\{1 - W(h/\ell) : h \geq 1\}$ and $\{\|\widehat{C}_{X,h}\|_2 : h \geq 1\}$. See, e.g., Rice and Shang (2017) for the selection of bandwidth ℓ .

Denote $T_N^o(\theta)$ to be the projection-based test statistics based on the eigenfunctions of $\mathcal{LC}_X(\cdot)$. The following theorem states that the empirical test statistic $\widetilde{T}_N(\theta)$ uniformly converges to $T_N^o(\theta)$ in distribution under H_0 , namely, $\widetilde{T}_N(\theta) \xrightarrow{d} \sup_{\theta \in (0,\theta)} \sum_{d=1}^D \tau_d B_d^2(\theta)$.

Theorem 3. Under Assumption 1 and H_0 , if $N^{-r_0} \sum_{d=1}^D \delta_{\tau,d}^{-1} \rightarrow 0$, then uniformly for $\theta \in (0, 1)$, $\widetilde{T}_N(\theta) \xrightarrow{d} T_N^o(\theta)$, where $\delta_{\tau,1} = \tau_1 - \tau_2$, $\delta_{\tau,d} = \max\{\tau_{d-1} - \tau_d, \tau_d - \tau_{d+1}\}$ for $d \geq 2$.

3.1.2 Identifiability of the Selected Basis Functions

Under H_a , the non-zero enhancement term $\rho\delta(t)\delta(s)$ is tuned through the tuning parameter ρ , and the identifiability of $K^{(\kappa)}(t, s)$ might be violated if ρ is not selected judiciously. Herein, in addition to the selection discussed in the previous section, we propose to tune ρ so that the identifiability of the eigenfunctions $\{\psi_d^{(\kappa)}(t) : d \geq 1\}$ is asymptotically guaranteed. Since $LC_{Y,\kappa}(t, s)$ and $LC_Y(t, s)$ are positive definite, by Mercer's theorem, we can find a sequence of positive values and orthonormal basis functions for each of them so that,

$$LC_{Y,\kappa}(t, s) = \sum_{d \geq 1} \lambda_d^{(\kappa)} \nu_d^{(\kappa)}(t) \nu_d^{(\kappa)}(s), \quad LC_Y(t, s) = \sum_{d \geq 1} \lambda_d \nu_d(t) \nu_d(s).$$

Since $LC_{Y,\kappa}(t, s) \rightarrow LC_Y(t, s)$ under H_a , the identifiability of $\{\theta_d^{(\kappa)} : d \neq d^*\}$ is guaranteed as $\kappa \rightarrow 0$ given the identifiability of $\{\lambda_d : d \geq 1\}$. Thus the identifiability of $\psi_{d^*}^{(\kappa)}(t)$ is of major interest here. We propose that the selected ρ is adjusted so that $\rho\|\hat{\delta}\|^2$ lies in the middle of the two neighboring eigenvalues of $\widehat{\mathcal{LC}}_{Y,\kappa}(\cdot)$. If $\rho\|\hat{\delta}\|^2$ is greater than the maximal eigenvalue of $\widehat{\mathcal{LC}}_{Y,\kappa}(\cdot)$, then ρ is selected so that $\rho\|\hat{\delta}\| - \hat{\lambda}_1^{(\kappa)}$ is greater than a non-trivial positive constant L_ρ , e.g., $\hat{\lambda}_1^{(\kappa)} - \hat{\lambda}_2^{(\kappa)}$. It can be shown that the identifiability of $\psi_{d^*}^{(\kappa)}(t)$ is asymptotically guaranteed under some mild conditions. To justify this, we first introduce the following assumptions.

Assumption 4. The eigenvalues $\{\lambda_d : d \geq 1\}$ satisfy the conditions $R^{-1}d^{-\alpha_\theta} \leq \lambda_d \leq Rd^{-\alpha_\theta}$, where R is a positive constant, and $\lambda_d - \lambda_{d+1} \geq \text{const.}d^{-\alpha_\theta-1}$. In addition, $\rho = O(N^\beta)$, and $\|\delta\| = O(N^{\alpha_\delta})$, where $\alpha_\delta > -1/2$.

Assumption 4 quantifies the decay rate of eigenvalues $\{\lambda_d : d \geq 1\}$ and restricts the spacing of eigenvalues from being overly small, which enables the identifiability of $\{\lambda_d : d \geq 1\}$ (see also Cai and Hall (2006)). It is required that $\alpha_\delta > -1/2$ because $\|\hat{\delta} - E\hat{\delta}\| = O_p(N^{-1/2})$. If $\|\delta\|$ decays faster than the estimation error, it is impossible to detect the change. Note that $d^* = O((\rho\|\delta\|^2)^{-1/\alpha_\theta})$ under Assumption 4.

Theorem 4. Under Assumption 4 and H_a , if $D^{\alpha_\theta+1}N^{-r_a} \rightarrow 0$, asymptotically almost surely, $\theta_{d^*}^{(\kappa)}$ is the only value between θ_{d^*-1} and θ_{d^*+1} . In addition, if $D(\rho\|\delta\|^2)^{1/\alpha_\theta} \rightarrow \infty$, then for arbitrary $\epsilon > 0$, $\max\{\theta_{d^*-1} - \theta_{d^*}^{(\kappa)}, \theta_{d^*}^{(\kappa)} - \theta_{d^*+1}\} \geq (\theta_{d^*-1} - \theta_{d^*+1})/(2 + \epsilon)$ or $\theta_1^{(\kappa)} - \theta_2 \geq L_\rho/(1 + \epsilon)$ as $d^* = 1$ asymptotically almost surely.

Theorem 4 demonstrates that the eigenvalue spacing $\max\{\theta_{d^*-1} - \theta_{d^*}^{(\kappa)}, \theta_{d^*}^{(\kappa)} - \theta_{d^*+1}\}$ is sufficiently large asymptotically almost surely, and consequently the identifiability of the jump-aligned basis is guaranteed as $N \rightarrow \infty$.

3.1.3 Selection of D

Cumulative percentage of variance is a widely accepted criterion for the selection of dimension, and is adjusted for the selection of D in the new method. In principle, the selection of D should lead to a sufficient portion of explained variation, and enhance the possibility that the jump function $\delta(t)$ is well aligned with the selected basis functions.

Define

$$R_\lambda(D) = \sum_{d=1}^D \hat{\lambda}_d^{(\kappa)} \Big/ \sum_{d \geq 1} \hat{\lambda}_d^{(\kappa)}, \quad (3-1)$$

γ is a positive constant taking the value, e.g., 80%–90%, and D_{pre} as the minimal value of D satisfying $R_\lambda(D) \geq \gamma$, and \hat{d}^* as the maximal value of d satisfying $\hat{\lambda}_d^{(\kappa)} > \rho\|\hat{\delta}\|^2$. Two scenarios are considered:

- (1) if $\rho\|\hat{\delta}\|^2 > \hat{\lambda}_{D_{pre}}^{(\kappa)}$, set $D = D_{pre} + d_\epsilon$,

(2) if $\rho\|\hat{\delta}\|^2 \leq \hat{\lambda}_{D_{pre}}^{(\kappa)}$, set $D = \hat{d}^* + d_\epsilon$,

where d_ϵ is some small-valued positive integer. Now we give the reasoning of the selection. Condition (1) is important in controlling the size of the test. Note that $\hat{\delta}(t)$ is always non-zero even under H_0 . As an extreme case, if $\hat{\delta}(t)/\|\hat{\delta}\|$ is the only incorporated basis function, the detector always tends to detect a change point and thus the type-I error can be extremely high, because the estimation errors falsely favor a change-point under H_0 . To attenuate such “over-enhancement” effect, it is necessary to incorporate multiple basis functions that capture sufficient variation to mitigate the estimation uncertainty of $\hat{\delta}(t)$. Condition (2) substantially increases the chance that the jump-aligned basis $\psi_{d^*}^{(\kappa)}$ is selected due to the fact $\hat{\theta}_d^{(\kappa)} \xrightarrow{p} \theta_d$, and is important in solving the “non-alignment” problem in projection-based detector. It can be obtained from Theorem 4 that, with such selection of D , the jump-aligned basis is selected asymptotically almost surely.

3.2 Power Studies

This section presents the asymptotic properties of the enhanced detector and the detection power. It has already been shown in the existing literature that, as the jump function is fixed and the selected basis functions are aligned with the jump in mean, the power of CUSUM-type detector approaches one as the sample size goes to infinity. However, it has not been studied under what conditions the asymptotically perfect detector (with power approaching one) can be achieved in a more general setting. In contrast, the dimension D , the magnitude of jump $\|\delta\|$, and the tuning parameter ρ are all allowed to vary with the sample size N here. To present the theoretical results under this general setting, we first introduce the function

$$V(\theta) = \begin{cases} \theta(1 - \theta^*), & 0 < \theta \leq \theta^*, \\ \theta^*(1 - \theta), & \theta^* < \theta < 1. \end{cases}$$

The following theorem presents the conditions that guarantee the convergence of the test statistic $\tilde{T}_N(\hat{\theta}_N^*)$ and also the convergence rate.

Theorem 5. Under Assumption 1—4 and H_a , define $r_\delta = \max\{\alpha_\ell - \alpha_\kappa - \alpha_\delta - 1/2, \alpha_\delta + \beta - 1/2\}$ and $U_N = \max\{D^{1/2}(\rho\|\delta\|^2)^{-1}, N^{r_\delta-r_a}(\rho\|\delta\|^2)^{-(1+1/\alpha_\theta)}, N^{r_\delta-1/2}\}$, if $D^{\alpha_\delta+3/2}/N^{r_a} \rightarrow 0$ and $D(\rho\|\delta\|^2)^{1/\alpha_\theta} \rightarrow \infty$, then

$$\sup_{\theta \in (0,1)} \left| N^{-1} \tilde{T}_N(\theta) - \|\delta\|^2 V^2(\theta) \right| \leq O_p(N^{-r_\delta}) \|\delta\| U_N.$$

Since it is assumed that $\alpha_\delta > -1/2$, $N\|\delta\|^2 \rightarrow \infty$ as $N \rightarrow \infty$. The theorem demonstrates that the convergence rate of $N^{-1} \tilde{T}_N(\theta)$ is uniformly bounded by $N^{-r_\delta} \|\delta\| U_N$. Therefore, if the ratio $N^{-r_\delta} \|\delta\| U_N / \|\delta\|^2$ converges to zero, it is sufficient to conclude that $\tilde{T}_N(\theta) \xrightarrow{p} N\|\delta\|^2 V^2(\theta)$.

The following corollary presents the regularity conditions that guarantees the detection power approaching one.

Corollary 1. Under Assumption 1—4 and H_a , if the conditions in Theorem 5 hold, and $N^{-r\delta} \|\delta\|^{-1} U_N \rightarrow 0$, then $\Pr(H_0 \text{ is rejected} | H_a) \rightarrow 1$. In addition, $\hat{\theta}_N \xrightarrow{p} \theta^*$.

The first part of the corollary can be obtained from Theorem 5 and the fact that $\tilde{T}_N(\theta) \xrightarrow{p} \infty$ under H_a . This corollary demonstrates that, the detection power will approach one if the magnitude $\|\delta\|^2$ decays slower than the convergence rate of $N^{-1}\tilde{T}_N(\theta)$. The consistency of $\hat{\theta}_N$ can be obtained by the continuous mapping theorem of argmax function and the fact that θ^* is the unique maximizer of $V(\theta)$.

4 Simulation

4.1 General Setting

Finite sample properties are investigated in this section. First, $N = 200$ or $N = 400$ innovation functions are generated over the unit interval $[0, 1]$ with $B = 20$ Fourier basis functions $\{F_6(t), \dots, F_{25}(t)\}$ specified as follows

$$F_i(t) = \begin{cases} 1, & \text{if } i = 1. \\ \sqrt{2} \cos(2\pi kt), & \text{if } i = 2k. \\ \sqrt{2} \sin(2\pi kt), & \text{if } i = 2k + 1. \end{cases}$$

The change in functional means is located in the middle of the sequence and is driven by the 2nd Fourier basis, which is orthogonal to the 20 basis functions used to generate the innovations. The functions are simulated by the following basis expansion contaminated by random noises $\{\epsilon_n(t_j) : n = 1, \dots, N, j = 1, \dots, T\}$

$$X_n(t_j) = \begin{cases} \sum_{d=1}^B \xi_{nd} F_{d+5}(t_j) + \epsilon_n(t_j), & 1 \leq n \leq \lfloor N/2 \rfloor, j = 1, \dots, T \\ \sum_{d=1}^B \xi_{nd} F_{d+5}(t_j) + \delta(t_j) + \epsilon_n(t_j), & \lfloor N/2 \rfloor + 1 \leq n \leq N, j = 1, \dots, T, \end{cases}$$

where $\epsilon_n(t_j) \stackrel{i.i.d.}{\sim} \mathcal{N}(0, s^2)$, and $t_j = j/100$, $T = 100$. We set $\delta(t) = aF_2(t)$, where $a = 0$ under H_0 and $a > 0$ under H_a . To highlight the effect of the magnitude $\|\delta\|$, different values of a are considered. The variation of random errors $\{\epsilon_n(t_j) : t_j = 1, \dots, T, n \geq 1\}$ is tuned through s . The obtained functions are smoothed with the first 35 Fourier basis functions.

Define $\boldsymbol{\sigma} = \{1.2^{-2d} : d = 1, \dots, B\}$. Two distributional setup of $\boldsymbol{\xi}_n = (\xi_{n1}, \dots, \xi_{nB})$ are considered, namely, $\{\boldsymbol{\xi}_n : n \geq 1\}$ are

1. (Independent case) *i.i.d.* random vectors following the distribution $\mathcal{N}(0, \boldsymbol{\sigma})$.
2. (Dependent case) a FMA(3) process $\boldsymbol{\xi}_n = \sum_{j=1}^3 \Phi_j \mathbf{e}_{n-j} + \mathbf{e}_n$, where $\mathbf{e}_n \sim \mathcal{N}(0, \boldsymbol{\sigma})$, $\Phi_1(\cdot) = 0.6\mathbf{I}(\cdot)$, $\Phi_2(\cdot) = 0.4\mathbf{I}(\cdot)$, $\Phi_3(\cdot) = 0.2\mathbf{I}(\cdot)$ and $\mathbf{I}(\cdot)$ is the identity operator.

Here we set $\gamma = 90\%$. The enhancement parameters considered are $\rho_1 = N^{0.25}$, $\rho_2 = N^{0.3}$, $\rho_3 = N^{0.35}$, and $\rho_4 = N^{0.40}$. We use the R package *sde* to simulate the null distribution, and the simulations are run with the same seeds under different settings. The proposed detector is compared with two other representative competitors in functional change-point problem: fPC-based approach (see e.g., Berkes *et al.* (2009)) and fully functional approach (see e.g., Aue *et al.* (2018)). For the fPC-based detector, the dimension is selected so that the incorporated functional principal components explain 90% of the total variation.

4.2 Spectral Distribution of $LC_X(t, s)$

As discussed, the enhanced procedure can reduce the nuisance effect of irrelevant basis functions that are not aligned with the change, and the improvement in detection power is substantial especially when the functions cannot be well explained by a small number of basis functions or are contaminated by random errors. In fact, these two cases are sometimes related. If the functions are contaminated by random noises, it is typically necessary to incorporate more basis to explain the noisy functions sufficiently.

To visualize the relation between the spectra of the (long-run) covariance function $LC_X(t, s)$ and the standard deviation of random error s , we study the decay rate of the (scaled) eigenvalues $\{\tau_d/\tau_1: d \geq 1\}$ under different values of s and display the results in Figure 1. Here the estimated (long-run) covariance function $\widehat{LC}_X(t, s)$ are obtained from 2000 simulated innovation functions.

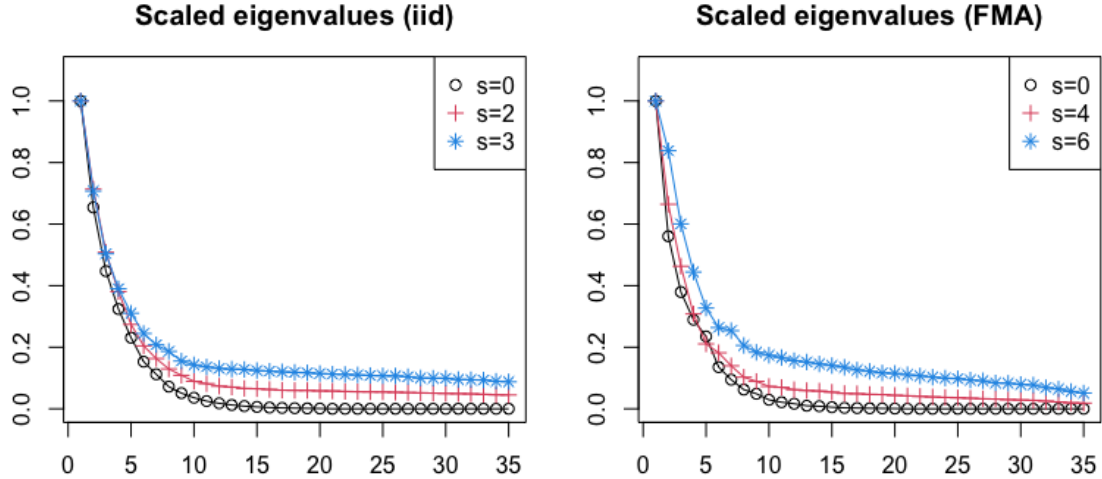


Figure 1: Scaled eigenvalues of the (long-run) covariance function $\widehat{LC}_X(t, s)$. Left panel: Setting 1 (*i.i.d.* sequence), $s = 0, 2, 3$; Right panel: Setting 2 (FMA(3) process), $s = 0, 4, 6$.

Clearly, as the variation of random error increases, the decay rate of spectra decreases. This is because random errors bring more complicated variation pattern, and thus more functional principal components have to be incorporated to explain the contaminated functions sufficiently. Since the random errors are not informative to the change function $\delta(t)$, if the basis functions are not carefully selected or overly many basis are selected, the power of the detection will be reduced by the nuisance effect of the irrelevant basis functions, see Section 4.3.

4.3 Empirical Size and Power

In this section, we compare the empirical size and power of the three methods under the setting that there exists a single change point in the middle. In each setting, the simulation runs are repeated for 5000 times under nominal level 0.05, and the empirical sizes and powers are reported in Table 1 for setting 1 and Table 2 for setting 2.

It can be seen that as the variation of random error increases, the superiority of the developed enhanced detector becomes more pronounced. This numerically justifies that the proposed detector can attenuate the nuisance effect of random error or irrelevant basis functions. In addition, the size and power of the proposed method is robust to the selection of the enhancement parameter ρ . The ordinary functional principal components are not very reliable and the detection are not robust to random noises. The fully functional approach, though performs better than the fPC-based approach, still gives suboptimal performance compared to the our new approach.

Table 1: Empirical sizes and powers under different values of a and s (i.i.d.).

| a | N | s | DECP | | | | FF | fPC |
|------|-----|-----|----------|----------|----------|----------|-------|-------|
| | | | ρ_1 | ρ_2 | ρ_3 | ρ_4 | | |
| 0.00 | 200 | 0.5 | 0.056 | 0.057 | 0.057 | 0.058 | 0.056 | 0.048 |
| | | 1.0 | 0.057 | 0.058 | 0.057 | 0.057 | 0.057 | 0.046 |
| | | 1.5 | 0.057 | 0.057 | 0.057 | 0.058 | 0.052 | 0.047 |
| | 400 | 0.5 | 0.047 | 0.049 | 0.049 | 0.049 | 0.053 | 0.049 |
| | | 1.0 | 0.054 | 0.055 | 0.055 | 0.056 | 0.050 | 0.049 |
| | | 1.5 | 0.061 | 0.058 | 0.058 | 0.059 | 0.050 | 0.044 |
| 0.20 | 200 | 0.5 | 0.147 | 0.149 | 0.147 | 0.149 | 0.145 | 0.055 |
| | | 1.0 | 0.139 | 0.139 | 0.139 | 0.140 | 0.126 | 0.073 |
| | | 1.5 | 0.141 | 0.143 | 0.143 | 0.144 | 0.126 | 0.103 |
| | 400 | 0.5 | 0.406 | 0.404 | 0.403 | 0.396 | 0.363 | 0.056 |
| | | 1.0 | 0.400 | 0.403 | 0.407 | 0.415 | 0.360 | 0.141 |
| | | 1.5 | 0.438 | 0.443 | 0.443 | 0.441 | 0.373 | 0.313 |
| 0.22 | 200 | 0.5 | 0.183 | 0.185 | 0.187 | 0.183 | 0.179 | 0.057 |
| | | 1.0 | 0.177 | 0.175 | 0.175 | 0.177 | 0.158 | 0.099 |
| | | 1.5 | 0.182 | 0.184 | 0.186 | 0.185 | 0.159 | 0.134 |
| | 400 | 0.5 | 0.603 | 0.598 | 0.595 | 0.588 | 0.544 | 0.058 |
| | | 1.0 | 0.591 | 0.590 | 0.596 | 0.607 | 0.537 | 0.289 |
| | | 1.5 | 0.619 | 0.625 | 0.621 | 0.623 | 0.550 | 0.481 |
| 0.24 | 200 | 0.5 | 0.239 | 0.239 | 0.239 | 0.239 | 0.232 | 0.060 |
| | | 1.0 | 0.231 | 0.231 | 0.233 | 0.233 | 0.207 | 0.144 |
| | | 1.5 | 0.235 | 0.236 | 0.237 | 0.237 | 0.209 | 0.183 |
| | 400 | 0.5 | 0.842 | 0.838 | 0.834 | 0.828 | 0.791 | 0.061 |
| | | 1.0 | 0.808 | 0.806 | 0.815 | 0.824 | 0.775 | 0.603 |
| | | 1.5 | 0.808 | 0.813 | 0.812 | 0.815 | 0.761 | 0.704 |

Table 2: Empirical sizes and powers under different values of a and s (FMA).

| a | N | s | DECP | | | | FF | fPC |
|------|-----|-----|----------|----------|----------|----------|-------|-------|
| | | | ρ_1 | ρ_2 | ρ_3 | ρ_4 | | |
| 0.00 | 200 | 2.0 | 0.055 | 0.056 | 0.056 | 0.055 | 0.053 | 0.022 |
| | | 3.0 | 0.052 | 0.053 | 0.052 | 0.053 | 0.050 | 0.021 |
| | | 4.0 | 0.053 | 0.053 | 0.054 | 0.053 | 0.047 | 0.022 |
| | 400 | 2.0 | 0.053 | 0.054 | 0.054 | 0.054 | 0.057 | 0.037 |
| | | 3.0 | 0.055 | 0.055 | 0.055 | 0.056 | 0.051 | 0.035 |
| | | 4.0 | 0.049 | 0.050 | 0.051 | 0.050 | 0.047 | 0.032 |
| 0.40 | 200 | 2.0 | 0.124 | 0.123 | 0.123 | 0.122 | 0.114 | 0.056 |
| | | 3.0 | 0.117 | 0.117 | 0.118 | 0.119 | 0.108 | 0.054 |
| | | 4.0 | 0.116 | 0.115 | 0.115 | 0.114 | 0.099 | 0.051 |
| | 400 | 2.0 | 0.280 | 0.278 | 0.285 | 0.292 | 0.287 | 0.225 |
| | | 3.0 | 0.305 | 0.305 | 0.305 | 0.302 | 0.267 | 0.222 |
| | | 4.0 | 0.283 | 0.284 | 0.287 | 0.282 | 0.258 | 0.202 |
| 0.50 | 200 | 2.0 | 0.203 | 0.203 | 0.201 | 0.200 | 0.184 | 0.104 |
| | | 3.0 | 0.188 | 0.189 | 0.191 | 0.190 | 0.175 | 0.095 |
| | | 4.0 | 0.184 | 0.183 | 0.182 | 0.183 | 0.162 | 0.092 |
| | 400 | 2.0 | 0.660 | 0.660 | 0.660 | 0.666 | 0.667 | 0.592 |
| | | 3.0 | 0.685 | 0.688 | 0.685 | 0.671 | 0.614 | 0.566 |
| | | 4.0 | 0.632 | 0.636 | 0.641 | 0.626 | 0.582 | 0.507 |
| 0.60 | 200 | 2.0 | 0.363 | 0.361 | 0.358 | 0.361 | 0.328 | 0.222 |
| | | 3.0 | 0.344 | 0.342 | 0.341 | 0.337 | 0.313 | 0.201 |
| | | 4.0 | 0.331 | 0.329 | 0.332 | 0.329 | 0.291 | 0.189 |
| | 400 | 2.0 | 0.982 | 0.982 | 0.982 | 0.982 | 0.985 | 0.973 |
| | | 3.0 | 0.976 | 0.976 | 0.977 | 0.975 | 0.964 | 0.959 |
| | | 4.0 | 0.954 | 0.954 | 0.955 | 0.952 | 0.939 | 0.910 |

4.4 Variation of the Detected Change-points

To study the finite sample properties of the estimated change-point, we provide the box-plots of the estimated change-points in Figures 2–5. In each figure, there are six boxes. The first four boxes pertain to the proposed detector under $\rho = N^{0.25}$, $\rho = N^{0.3}$, $\rho = N^{0.35}$, and $\rho = N^{0.4}$ respectively. The 5th box pertains to the fully functional detector and the last one pertains to the fPC-based approach.

Overall, the variance of the estimated change-points of the proposed detector and the fully functional detector are similar, and that of the fPC-based procedure can be sometimes much higher. It is also noted that the variance of the change point estimator of the proposed detector is robust to the selection of ρ .

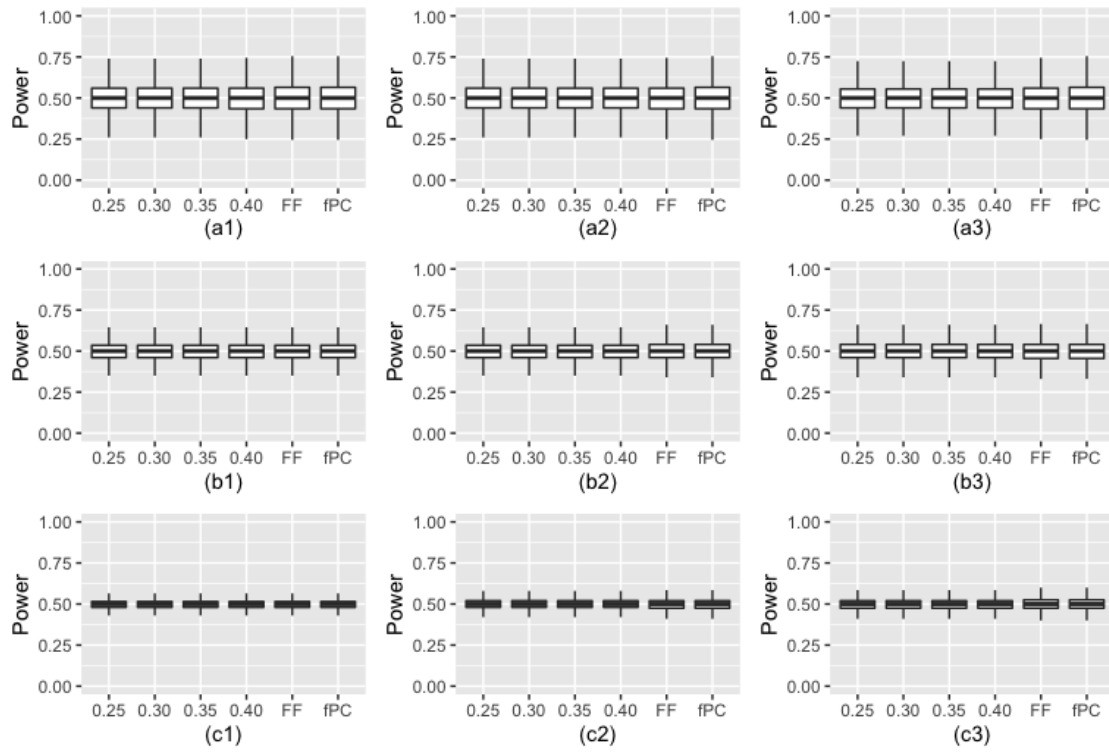


Figure 2: Box-plots of detected change-points (N=200, FMA).

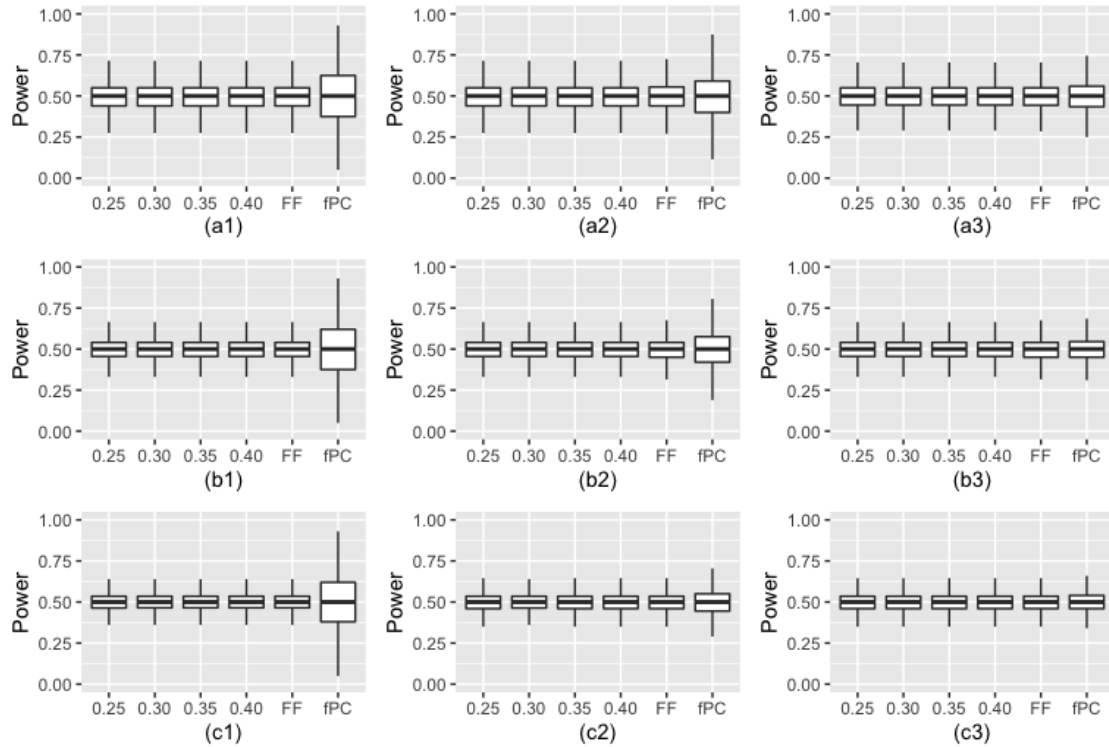


Figure 3: Box-plots of detected change-points (N=200, i.i.d.).

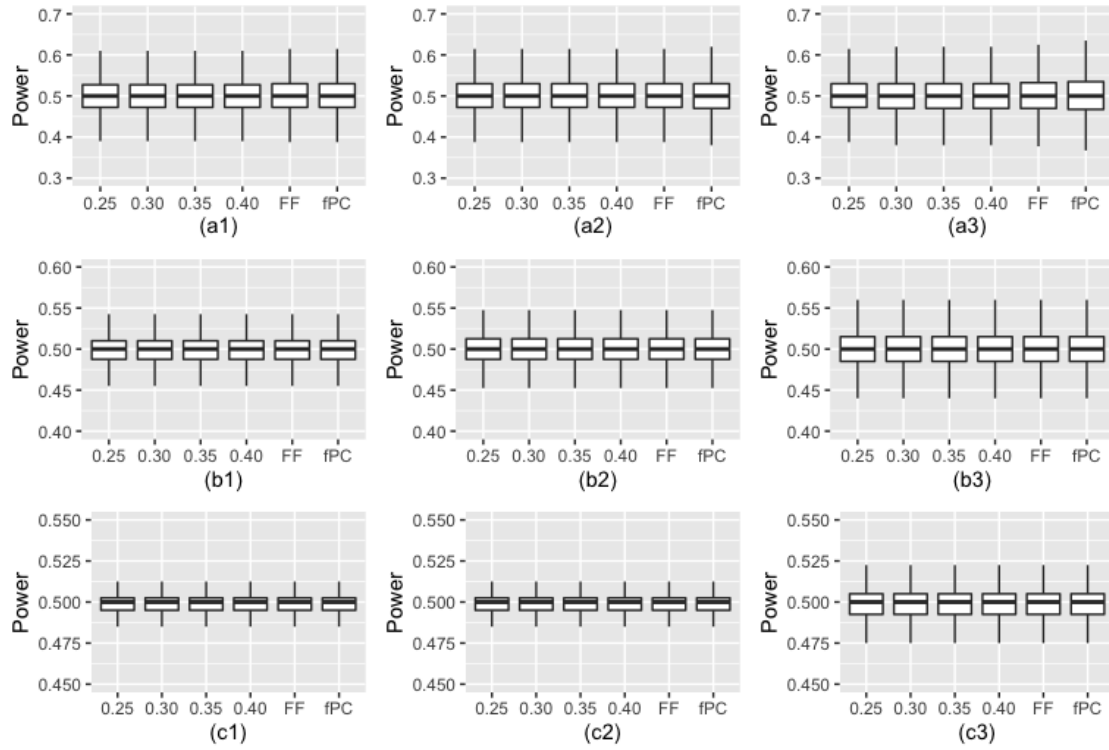


Figure 4: Box-plots of detected change-points (N400, FMA).

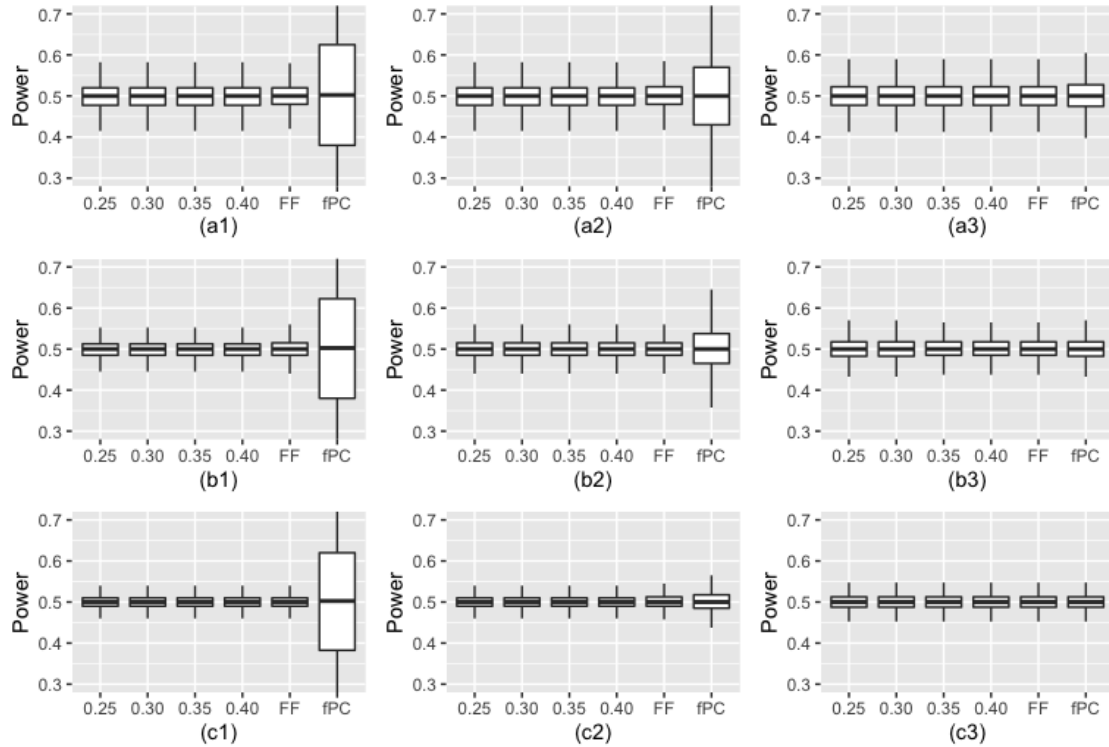


Figure 5: Box-plots of detected change-points (N=400, i.i.d.).

The simulations results are summarized as follows.

1. The levels of the proposed detector is well controlled around the nominal level under both *i.i.d.* and dependent case.
2. The performance of the proposed detector is robust to the selection of ρ and random errors, while the other two competitors are evidently more sensitive to random errors.
3. The power of the proposed detector is substantially higher than that of both competitors especially when the noise variation is high. The fPC-based detector typically gave the worst performance. It numerically demonstrates the necessities of careful selection of basis functions.
4. An interesting phenomenon in the *i.i.d.* case is that as the standard error of random error s increases, the power of the fPC-based detector obviously increases. However, the variance of the detected change-points is much higher than that of the proposed detector and the fully functional detector. In addition, in the dependent case, the empirical size of the fPC-based detector is not close to the nominal one. Thus, the ordinary functional principal components are not always reliable in change-point detection for functional data.

5 Application to Annual Humidity Trajectories

In this section, the proposed approach is applied to daily humidity trajectories obtained in Basel-City, Switzerland in 2021. The raw data consist of $N = 365$ daily measurements of humidity recordings (one observation per hour, 24 observations for each day) that are converted into functional objects by using 24 Fourier basis functions. The data can be downloaded at www.meteoblue.com. Figure 6 displays the trajectories.

For comparison, the proposed detector and the other two competitors (fPC-based detector and fully functional detector) are applied to date the time of the structural breaks. Here, $\gamma = 90\%$. For the fPC-based detector, the dimension is selected so that the incorporated functional principal components explain 90% of the total variation.

5.1 Dynamic Segmentation

To attenuate the violation of at most one change-point assumption (AMOC), we first segment the entire sequence into multiple disjoint blocks. The segmentation approach employed here is motivated by the dynamic segmentation approach (see Chiou *et al.* (2019)) and is adapted for our own purpose, which is described below.

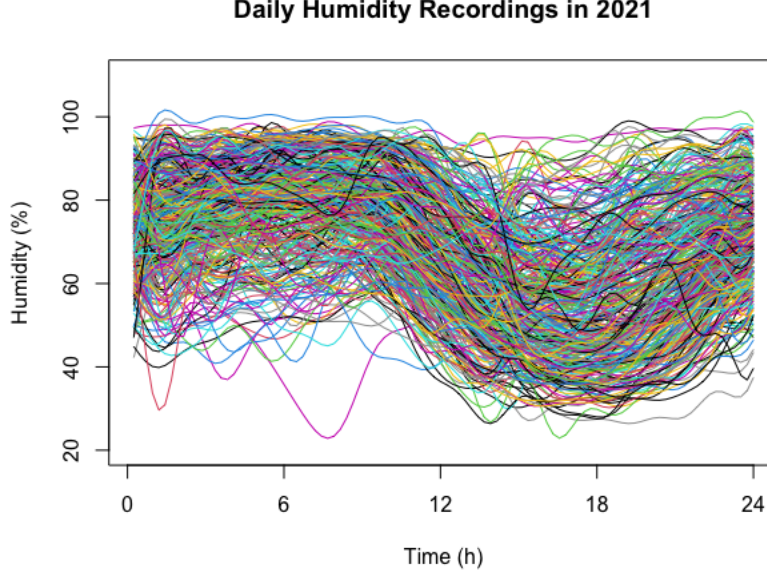


Figure 6: Daily humidity curves in Basel-City, Switzerland.

First we segment the whole functional sequences into 10 equal-length blocks

$$\{[\theta_r^{(0)}, \theta_{r+1}^{(0)}]: r = 1, \dots, 10\},$$

where $\theta_1^{(0)} = 1$ and $\theta_{11}^{(0)} = 365$. Then recursively update the segment points as follows.

Given a subinterval $[\theta_r, \theta_{r+1})$ of $[0, 365]$ and any θ in the subinterval, the sample covariance is calculated as follows

$$S_{[\theta_r, \theta_{r+1}]}^{(\theta)}(t, s) = \frac{1}{[N\theta_{r+1}] - [N\theta_r]} \sum_{n=[N\theta_r]}^{[N\theta_{r+1}]} \{X_n(t) - \bar{X}_n^{(\theta)}(t)\} \{X_n(s) - \bar{X}_n^{(\theta)}(s)\}$$

where

$$\bar{X}_n^{(\theta)}(t) = \begin{cases} \frac{1}{[N\theta] - [N\theta_r]} \sum_{n=[N\theta_r]}^{[N\theta]} X_n, & n \in [N\theta_r, N\theta] \\ \frac{1}{[N\theta_{r+1}] - [N\theta]} \sum_{n=[N\theta]+1}^{[N\theta_{r+1}]} X_n, & n \in (N\theta, N\theta_{r+1}]. \end{cases}$$

Suppose in the i -th iteration, the segmentation points are $\{[\theta_r^{(i)}, \theta_{r+1}^{(i)}]: r = 1, \dots, 10\}$, where $\theta_1^{(i)} = 1$ and $\theta_{11}^{(i)} = 365$ for all iteration i . For each $r > 1$, find the $\theta \in [\theta_{r-1}^{(i+1)}, \theta_{r+1}^{(i)}]$ that minimizes $\|S_{[\theta_{r-1}^{(i+1)}, \theta_{r+1}^{(i)}]}^{(\theta)}\|_{\mathcal{S}}$, which is set as $\theta_r^{(i+1)}$. The iteration stops when $\max_{1 \leq r \leq 13} |\theta_r^{(i+1)} - \theta_r^{(i)}| < 1/N$. The final segmentation points are denoted by $\{\tilde{\theta}_r, r = 1, \dots, 10\}$, where $\tilde{\theta}_1 = 1$ and $\tilde{\theta}_{11} = 365$.

Our proposal is that the whole sequence $[1, N]$ is segmented by $\{(\tilde{\theta}_r + \tilde{\theta}_{r+1})/2: r \geq 2\}$. Note that, in Chiou *et al.* (2019), $\{\tilde{\theta}_r, r = 2, \dots, 10\}$ are considered as change-

point candidates. Each candidate will be tested under the AMOC assumption, and the statistically nonsignificant ones are removed. Here we divide the sequence $[1, N]$ disjointly so that each segment contains one such candidate. The initial segmentation of $[1, 365]$ is displayed in Figure 7.

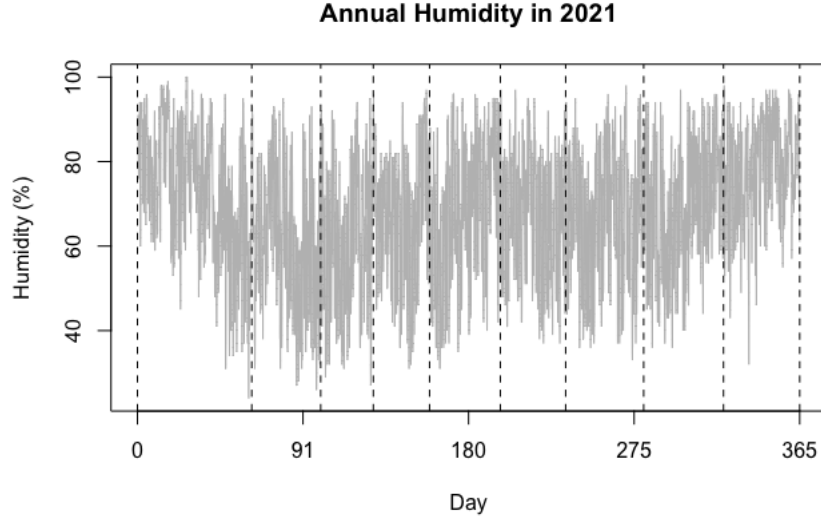


Figure 7: Initial segmentation.

5.2 Backward Elimination

For each segment, we apply the three detectors considered in the simulation to detect and date the change-point under the AMOC assumption. If there is no change point detected in the subinterval $[\theta_r, \theta_{r+1}]$, then remove θ_{r+1} and test the change-point in the longer subinterval $[\theta_r, \theta_{r+2}]$. The elimination procedure stops till no segmentation point is removed.

Here, $\ell = 3$, and $\rho = N^{0.4}$. Both our approach and the fully functional approach detected 4 change-points at nominal level 0.05, which are displayed in Figure 8, while the fPC-based approach detected two change-points only, say, the 43th and 304th day of the year. The mean functions of the 5 segments are displayed in Figure 9.

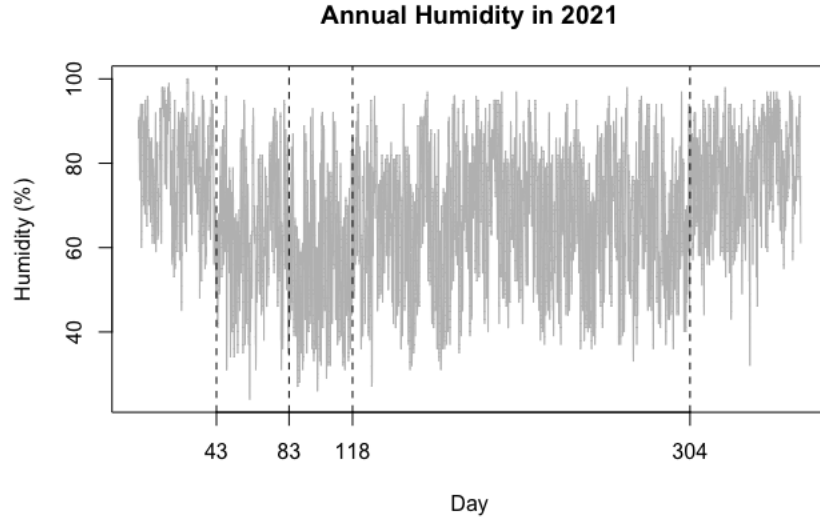


Figure 8: Detected days of change-points.

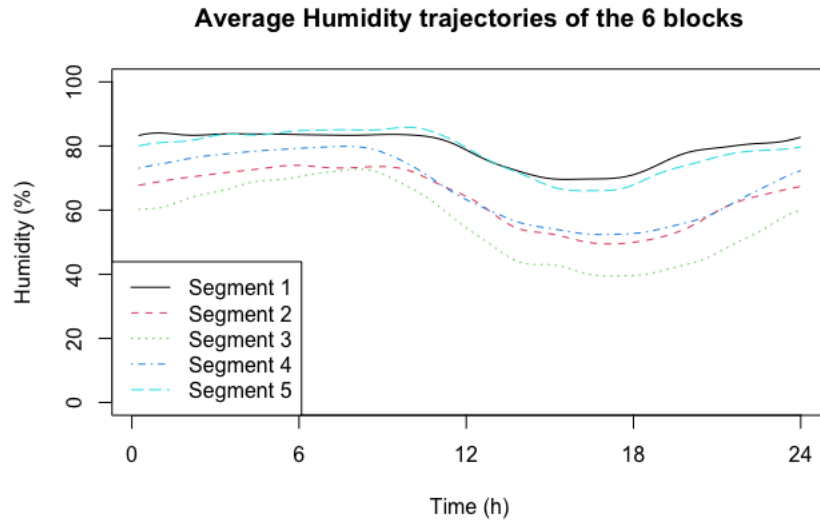


Figure 9: Average Humidity Trajectories of each segment.

In this application, although the proposed detector and the fully functional detector work similarly, there are cases when our approach is substantially superior to the fully functional approach. In the situation where the eigenvalues of the (long-run) covariance of functional sequence decays slowly, or the data are contaminated by random noise, there is evidence to believe that the developed procedure offers a more reliable means to detect the change-point.

6 Conclusions

In this paper, a new projection-based detector is introduced to detect and date the structural breaks in mean function for weakly dependent functional data. Theoretical results are developed under the assumption that both the magnitude of change and dimension vary with the sample size. This detector is developed to solve the limitations of two representative approaches, namely, fPC-based detector and fully functional detector. Specifically, the fPC-based approach cannot work while the employed fPCs fail to explain the structural breaks, and the fully functional approach essentially selects all basis functions that span the functional space, and thus suffers more from the nuisance effect of the irrelevant basis functions than the developed enhanced procedure. The proposed detector relies on the carefully selected basis functions that is informative to the change in mean, making it more reliable to detect the change while controlling the test size close to the nominal level. In the simulation study, it is shown that the proposed detector performs better than fully functional and fPC-based detector, especially when the spectra of the (long-run) covariance function decay slowly or the functions are substantially contaminated by random errors.

References

ASTON, J. A. & KIRCH, C. (2012a). Detecting and estimating changes in dependent functional data. *Journal of Multivariate Analysis* **109**, 204–220.

ASTON, J. A. & KIRCH, C. (2012b). Evaluating stationarity via change point alternatives with applications to fMRI data. *The Annals of Applied Statistics* **6**, 1906–1948.

AUE, A., GABRYS, R., HORVÁTH, L. & KOKOSZKA, P. (2009). Estimation of a change point in the mean function of functional data. *Journal of Multivariate Analysis* **100**, 1043–1073.

AUE, A., HÖRMANN, S., HORVÁTH, L. & HUŠKOVÁ, M. (2014). Dependent functional linear models with applications to monitoring structural change. *Statistica Sinica* **100**, 2254–2269.

AUE, A., HÖRMANN, S., HORVÁTH, L. & REIMHERR, M. (2009). Break detection in the covariance structure of multivariate time series models. *The Annals of Statistics* **37**, 4046–4087.

AUE, A., RICE, G. & SÖNMEZ, O. (2020). Structural break analysis for spectrum and trace of covariance operators. *Environmetrics* **31**, e2617.

AUE, A., RICE, G. & SÖNMEZ, O. (2018). Detecting and dating structural breaks in functional data without dimension reduction. *Journal of the Royal Statistical Society: Series B (Statistical Methodology)* **80**, 509–529.

AUE, A. & VAN DELFT, A. (2020). Testing for stationarity of functional time series in the frequency domain. *The Annals of Statistics* **48**, 2505–2547.

BERKES, I., GABRYS, R., HORVÁTH, L. & KOKOSZKA, P. (2009). Detecting changes in the mean of functional observations. *Journal of the Royal Statistical Society: Series B (Statistical Methodology)* **71**, 927–946.

BUCCIA, B. & WENDLER, M. (2017). Change-point detection and bootstrap for Hilbert space valued random fields. *Journal of Multivariate Analysis* **155**, 344–368.

CAI, T.-T. & HALL, P. (2006). Prediction in function linear regression. *The Annals of Statistics* **34**, 2159–2179.

CHIOU, J.-M., CHEN, Y.-T., & HSING, T. (2019). Identifying multiple changes for a functional data sequence with application to freeway traffic segmentation. *The Annals of Applied Statistics* **13**, 1430–1463.

FREMDT, S., HORVÁTH, L., KOKOSZKA, P. & STEINEBACH, J. (2014). Functional data analysis with an increasing number of projections. *Journal of Multivariate Analysis* **124**, 313–332.

GOHBERG, I., GOLDBERG, S. & Kaashoek, M. A. (1992). Operator Theory: Advances and Applications. *Classes of Linear Operators* **49**, Birkhäuser, Basel.

GROMENKO, O., KOKOSZKA, P. & REIMHERR, M. (2017). Detection of change in the spatiotemporal mean function. *Journal of the Royal Statistical Society: Series B (Statistical Methodology)* **79**, 29–50.

HORVÁTH, L., KOKOSZKA, P. & RICE, G. (2014). Testing stationarity of functional time series. *Journal of Econometrics* **179**, 66–82.

HÖRMANN, S., KIDZIŃSKI, L. & Hallin, M. (2015). Dynamic functional principal components. *Journal of the Royal Statistical Society: Series B (Statistical Methodology)* **77**, 319–348.

HÖRMANN, S. & KOKOSZKA, P. (2010). Weakly dependent functional data. *The Annals of Statistics* **38**, 1845–1884.

JARUŠKOVÁ, D. (2013). Testing for a change in covariance operator. *Journal of Statistical Planning and Inference* **143**, 1500–1511.

JIAO, S., FROSTIG, R. D. & OMBAO, H. (2022). Breaking Point Detection in Functional Covariance. *Scandinavia Journal of Statistics. doi.org/10.1111/sjos.12589*

RICE, G. & SHANG, H. L. (2017). A Plug-in Bandwidth Selection Procedure for Long-Run Covariance Estimation with Stationary Functional Time Series. *Journal of Time Series Analysis* **38**, 591–609.

SHARIPOV, O., TEWES, J. & WENDLER, M. (2016). Sequential block bootstrap in a Hilbert space with application to change point analysis. *Canadian Journal of Statistics* **44**, 300–322.

STOEHR, C., ASTON, J. A. & KIRCH, C. (2021). Detecting changes in the covariance structure of functional time series with application to fMRI data. *Econometrics and Statistics* **18**, 44-62.

TORGOVITSKI, L. (2015). Detecting changes in Hilbert space data based on “repeated” and change-aligned principal components. *arXiv preprint arXiv:1509.07409*

ZHANG, X., HAYHOE, K., WUEBBLES, D. & SHAO, X. (2010). Testing the structural stability of temporally dependent functional observations and application to climate projections. *Electronic Journal of Statistics* **5**, 1765–1796.